Brain Chemistry: How Does P450 Catalyze the O-Demethylation Reaction of 5-Methoxytryptamine to Yield Serotonin?

Patric Schyman, Dandamudi Usharani, Yong Wang, and Sason Shaik*

Institute of Chemistry and The Lise Meitner-Minerva Center for Computational Quantum Chemistry, The Hebrew University of Jerusalem, 91940 Jerusalem, Israel

Received: January 30, 2010; Revised Manuscript Received: March 27, 2010

Density functional theory has been applied to elucidate the mechanism of the O-demethylation reaction that generates serotonin from 5-methoxytryptamine (5-MT); a process that is efficiently catalyzed by P450 CYP2D6. Two substrates, the neutral 5-MT and the protonated 5-MTH$^+$, were used to probe the reactivity of CYP2D6 compound **I**. Notably, the H-abstraction process is found to be slightly more facile for 5-MT. However, our DFT augmented by docking results show that the amino acid Glu216 in the active site holds the NH_3^+ tail of the 5-MTH$^+$ substrate in an upright conformation and thereby controls the regioselectivity of the bond activation. Thus, the substrate protonation serves an important function in maximizing the yield of serotonin. This finding is in accord with experimental conclusions that 5-MTH$^+$ serves as the substrate for the CYP2D6 enzyme. The study further shows that the H-abstraction follows two-state reactivity (TSR), whereas the rebound path may involve more states due to the appearance of both Fe(IV) and Fe(III) electromers during the reaction of 5-MTH$^+$.

1. Introduction

Cytochrome P450 enzymes are most versatile biological catalysts[1,2] and are found in nearly all biological systems.[3−6] The mammalian P450 enzymes are of great interest since they dominate the metabolism of drugs.[7,8] One of the most interesting enzymes in this respect is CYP2D6, which is involved in the metabolism of almost one-third of all drugs on the market today.[9−11] This enzyme has been found in liver, heart, and brain tissues. Trace amines, such as tyramine and 5-methoxytryptamine are substrates to CYP2D6, which catalyzes their conversion to dopamine and serotonin. Serotonin is implicated in the creation of psychological balance, and malfunction in its production is for example responsible for depression and aggression.[12,13]

In addition, serotonin is converted into melatonin, and these two amines control the wake−sleep cycle. As can be seen from Scheme 1, CYP2D6 is involved in the last step of the cycle,[14] where serotonin is regenerated from 5-methoxytryptamine[15] (the neutral denoted 5-MT, and the protonated form denoted as 5-MTH$^+$), a metabolite and precursor of melatonin, via an O-demethylation reaction.

O-dealkylation is an intriguing reaction that can unmask a hydroxyl group and thereby activates the molecule.[16] This is of great biological interest, since it makes it possible for a chemical compound to be biologically inactive until it reaches its destination; in this case, the nerve cells. The possibility to activate a molecule at a desired location is a major challenge in developing new drugs for which the molecule must be transported through selection barriers, such as the blood−brain barrier, where an activated compound might not enter the brain. Our interest in the present paper is to elucidate the atomistic mechanism of the conversion of 5-MTH$^+$ to serotonin by P450.

Generally, three major types of mechanisms have been proposed for P450 oxidation reactions of organic molecules: (i) hydrogen atom transfer (HAT), followed by hydroxylation;[4,5] (ii) single electron transfer (SET), followed by a proton transfer; and (iii) direct oxo transfer to a π-bond or a heteroatom lone

SCHEME 1: The Serotonin-to-Melatonin Wake−Sleep Cycle

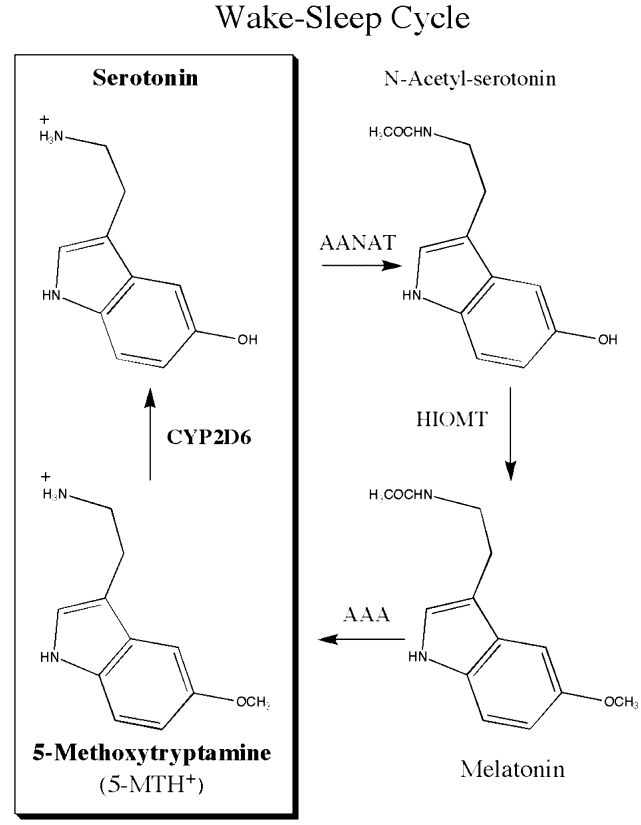

* Corresponding author. Fax: (+972)2-6584680. E-mail: sason@yfaat.ch.huji.ac.il.

10.1021/jp1008994
Published on Web 04/20/2010

SCHEME 2: The Overall Reaction for Serotonin Formation and the Proposed Reaction Mechanism

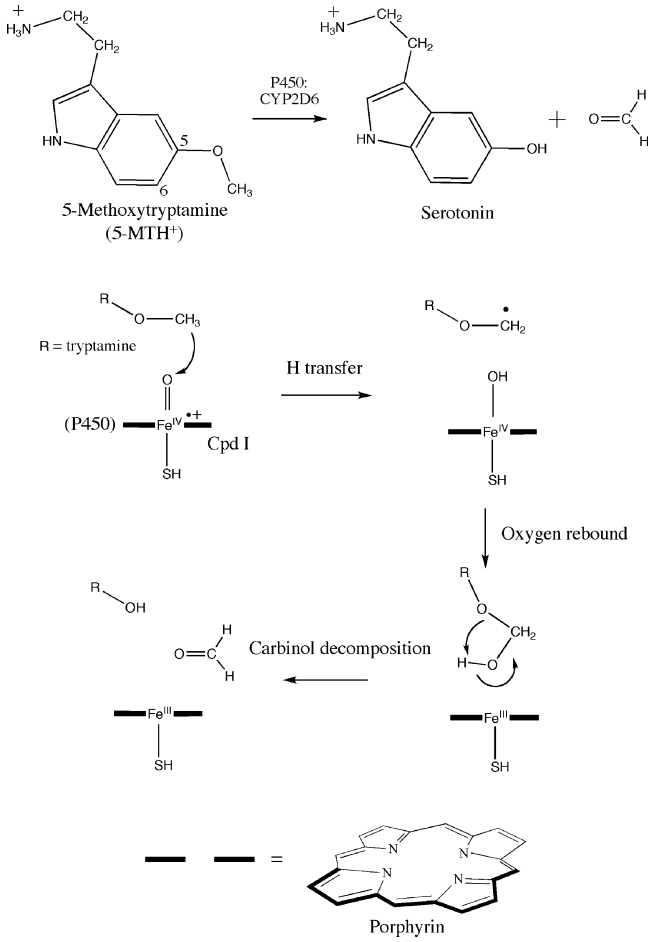

pair.[10,17] The SET mechanism has been proposed for the N-dealkylation[18,19] and in some S-dealkylation reactions;[20] however, the HAT mechanism for O-demethylation is supported by findings[20−22] of kinetic-isotope effect (KIE) values greater than 3, which correspond to a HAT rather than a stepwise mechanism with SET followed by a proton transfer that is normally expected to possess a small KIE value,[23−27] less than 2. The direct addition of the ferryl oxygen in the case of O-demethylation can be disregarded for the same reason that a high KIE would not be observed, or the observed value may even be the inverse, KIE < 1.

The HAT mechanism for the P450-catalyzed O-dealkylation is outlined in Scheme 2 and involves two processes. The first process, the hydroxylation reaction, is catalyzed by P450 and is initiated by a hydrogen atom transfer from the methyl group to the ferryl-oxo, followed by oxygen rebound to form a carbinol (hemiacetal) intermediate. The second process is the decomposition of the carbinol, leading to the demethylated product and a formaldehyde molecule. By analogy with the N-dealkylation process that generates formaldehyde, too, the second process may not occur in the active site of the enzyme.[28]

The different steps in the catalytic cycle of P450 and the manner whereby it performs hydroxylation reactions have been the subjects of many papers.[29−34] The P450 species that is believed to be involved in most hydroxylation reactions is the π-cation radical ferryl-oxo compound named compound I (Cpd I); see Scheme 2.[5,32−35] The different steps leading to Cpd I have been reviewed in several papers.[29−31] A key feature in the electronic structure of Cpd I is the a_{2u} orbital, which is a singly occupied orbital composed of a mixture of a porphyrin-based a_{2u} orbital and the thiolate ligand σ-hybrid pointing toward iron. This singly occupied orbital gives rise, therefore, to an almost degenerate high-spin (HS) quartet state and low-spin (LS) doublet state, depending on the spin orientation of the electron in the a_{2u} orbital. In most cases, the LS state is more reactive and has a somewhat lower barrier than the HS state.[30,36] In many cases, however, the two states are close and lead thereby to two-state reactivity (TSR) in which the product distribution is determined by both the LS and HS states.[30,37,38]

Despite many theoretical studies,[30] the mechanism of O-dealkylation catalyzed by P450 has not been studied before. This is done here using density functional theory (DFT) calculations of the formation of serotonin from 5-MTH$^+$ (Scheme 2). Under physiological conditions, the protonated form 5-MTH$^+$ has been identified as the substrate of CYP2D6.[39] The positively charged NH_3^+ group in the tail of the 5-MTH$^+$ could be crucial for binding the substrate in the active site due to the presence of negatively charged amino acids Glu216 and Asp301 that hold the substrate in position for the oxidation reaction.[40−45] In fact, the substrate has several oxidizable moieties, and yet, the reaction is selective for O-demethylation. Since the substrate-binding mode may affect the regioselectivity of the oxidation site, we study it herein using a docking procedure (see Methods). We note that the DFT calculations (below) show that the upright conformation, which is amenable only to O-demethylation, is the most stable conformer. As such, the docking calculations are meant to ascertain this QM result and verify whether the electrostatic interactions with the charge tail will further augment this preference for the upright conformation.

An argument for the importance of the charged amino group is that in some cases the neutral substrate has been found to act as an inhibitor.[21,46] Thus, in the study of dopamine formation,[46] in which the CYP2D6 is involved first in an O-demethylation reaction and then in a hydroxylation reaction, it was observed that as the concentration of neutral substrates increased after the first O-demethylation reaction, these substrates functioned as inhibitors for the second process. To verify whether the selection between 5-MTH$^+$ and 5-MT originates in their different reactivities or from their selective binding modes in the active site, we set out a DFT study for the hydroxylation in both protonation states and docking for substrate binding. In so doing, we hope to augment our DFT results by essential information regarding the role of the Asp301/Glu216 residues[47−49] in CYP2D6.

For completion, both the HS and LS states were investigated to probe the effect of selective spin state reactivity or a possible TSR scenario. In the carbinol decomposition step (Scheme 2), we explored the role of catalysis by 1−3 water molecules to complete the O-demethylation reaction.

2. Methods

Docking Calculations. Molecular docking was carried out on the CYP2D6 (2F9Q) X-ray crystal structure[49] using Autodock 4.02.[50] The substrates, the protein, and Cpd I were tested with different sets of charges, and we observe similar results. In a nutshell and irrespective of the charges used for the representation of the heme by oxoheme (Cpd I) or by the pentacoordinate species, *all the highly populated conformations of 5-MTH$^+$ were found to have the positive NH_3^+ tail pointing upward and held by the protein residues* by electrostatic and H-bonding interactions. These results were in contrast to *the unprotonated substrate, which preferred a conformation with the NH_2 tail pointing downward toward the heme* (Supporting Information

Figures S2−S4). The docking results obtained from a uniform set of Kollman charges are presented in the paper. The partial charges for Cpd I and heme[51,52] are taken from the literature. The details of protein and substrate (5-MTH$^+$, 5-MT) preparation for docking are given in the Supporting Information (SI). A GRID-based procedure was employed to prepare the structural input and to define the binding sites. A rectangular lattice (80 × 65 × 60 Å^3) with the grid center at the oxygen atom of Cpd I (−14.46, 51.083, −6.065) and with grid points separated by 0.375 Å was superimposed upon the entire protein structure. A Lamarckian genetic algorithm[53,54] was used for the search of 50 conformations, with all other parameters at their default settings. Resulting docked orientations within a root-mean-square deviation of 0.5 Å of each other were clustered together. For each substrate, the lowest energy conformation in each cluster was analyzed.

Electronic Structure Calculation. The methods and their reliability have been tested and demonstrated in previous papers[29,30,36] and will be briefly described here. Density functional theory calculations were carried out with Gaussian 03.[55] The $Fe^{4+}O^{2-}(C_{20}N_4H_{12})^-(SH)^-$ was used to model Cpd I of cytochrome P450,[56,57] and the 5-MTH$^+$ and 5-MT were taken in full as substrates. The spin-unrestricted B3LYP[58−60] was employed using two basis sets: (a) LACVP(Fe)/6-31G(rest), the so-called B1, to optimize the transition states and minima without symmetry constraints; and (b) a larger basis set, LACV3P+(Fe)/6-311++G**(rest), B2 in brief, for single-point energy calculations.[61,62] Stable species (minima, ground state) were shown to possess only positive vibrational frequencies, whereas transition states were ascertained to exhibit only one mode with an imaginary frequency. Bulk polarity effects of the active site in the protein environment were evaluated with the PCM solvation model using a nonpolar solvent (chlorobenzene, $\varepsilon = 5.62$). Single-point calculations were done also by including Glu216 in the quantum chemical model, and the results were very similar (see Table 3 and the Supporting Information) to those obtained by PCM calculations. The carbinol decomposition in the polar nonenzymatic environment was studied using an aqueous medium (water, $\varepsilon = 78.39$). The solvation cavity was created using the Pauling radii.

In the section for the oxygen rebound with Fe(III) and Fe(IV) species, we generated the Fe(III) from Fe(IV) by swapping the orbitals described in the Gaussian 03 manual. A vshift of 500 (Gaussian keyword to increase orbital energies) was used to sustain the desired electronic structure and thereby calculate the respective TS_{reb} energy with B1. During the subsequent calculations with B2, the vshift could be removed, leading therefore to more reliable B2 energies of these states. However, geometry optimization on this state ended up converging back on the Fe(IV) state, and therefore, in one case, there is a large gap between the ^{2,4}Fe(III) states, since one could be optimized but the other could not.

The KIE of the HAT process was determined using the Gaussian frequency data.[63] The procedure to calculate the KIE is described in a previous work including the Fortran code.[64] The semiclassical Eyring equation for calculating KIE is given as

$$\mathrm{KIE}_{\mathrm{Eyring}} = \left(\frac{k_\mathrm{H}}{k_\mathrm{D}}\right)_{\mathrm{Eyring}} = \exp\left[-\frac{\left(G_\mathrm{H}^{\neq} - G_\mathrm{H}^{\mathrm{R}}\right) - \left(G_\mathrm{D}^{\neq} - G_\mathrm{D}^{\mathrm{R}}\right)}{RT}\right] \quad (1)$$

where the k_H/k_D is the ratio between the reaction rates of hydrogen and deuterium abstraction, and $(G_H^{\neq} - G_H^R)$ is the free energy difference between the transition state and the reactant. The temperature in our calculations was 298.15 K. Equation 1 is multiplied by the Wigner correction factor, $Q_{\mathrm{Wigner}}^{\mathrm{corr}}$, for estimating tunneling effects:

$$\mathrm{KIE}_{\mathrm{Wigner}} = \left(\frac{k_\mathrm{H}}{k_\mathrm{D}}\right)_{\mathrm{Wigner}} = Q_{\mathrm{Wigner}}^{\mathrm{corr}}\left(\frac{k_\mathrm{H}}{k_\mathrm{D}}\right)_{\mathrm{Eyring}} \quad (2)$$

$$Q_{\mathrm{Wigner}}^{\mathrm{corr}} = \frac{1 + u_t^2/24}{1 + u'^2_t/24} \quad (3)$$

With $u_t^2 = h\upsilon_H/k_BT$ and $u'^2_t = h\upsilon_D/k_BT$ and υ is the imaginary frequency at the transition state. More details can be found in references 63 and 64. All the detailed data are collected in the Supporting Information.

3. Results

The mechanistic details of the O-demethylation reaction are described in three main sections. The first section, Substrate Docking, deals with the orientation of 5-MTH$^+$ vs 5-MT in the active site. The second, Hydroxylation, describes the hydroxylation reactions of 5-MTH$^+$ and 5-MT catalyzed by P450 forming a carbinol intermediate. The third section, Carbinol Decomposition, focuses on the decomposition of the carbinol intermediate to form the final product, serotonin, which is most likely not catalyzed by P450. The many data obtained in the study are available in the Supporting Information document, and the main text discusses the key results.

Substrate Docking. The reactant complex of P450 and the neutral 5-MT substrate can form two distinct geometries, with the substrate either lying flat over the heme (face-on) or standing in an upright position (side-on), with the oxidizable group oriented toward Cpd I. DFT calculations with 5-MT give both orientations for the 5-MT with slightly different preferences, depending on which basis set is used; B1 [LACVP(Fe)/6-31G(rest)] prefers the face-on conformation, and LACVP(Fe)/6-31G* favors the upright geometry (see Figure S1 in the Supporting Information). *However, the charged 5-MTH$^+$ always favors the upright position with the NH_3^+ tail pointing away from the heme, irrespectively of the basis set used.* To obtain additional information about substrate orientation, we performed docking calculations of the two substrates (further details of these calculations can be found in the Supporting Information).

Figure 1 shows the docking results of 5-MTH$^+$ in **1a** and of 5-MT in **2a** and **2b** (for other conformations, see Supporting Information Figures S2 and S3). No face-on conformation was found for either of the two substrates. The three most populated docking poses exhibited by 5-MTH$^+$ involve exclusively a binding mode with the NH_3^+ tail being held up and interacting with Glu216 (see **1b** and **1c**, Supporting Information Figure S2), which clearly favors O-demethylation. The most populated conformation of 5-MTH$^+$ (**1a**) has four types of interactions that buttress the upright (NH_3^+ up) conformation. They are (i) hydrogen bonding of the protonated amino group (NH_3^+) with Glu216 and Ser304; (ii) $\pi-\pi$ interactions of the indole ring with the Phe120 ring; (iii) weak interaction of the C−H bond of the OMe group with the oxygen atom of the Cpd I heme unit; and (iv) hydrophobic interactions of the planar aromatic ring with the Leu220, 213, and 484; and (v) electrostatic attractions with Glu216, and long-range interactions with Asp301 (Figure 1). These types of interactions are similar to other known amine substrates.[65−67] Further interacting residues

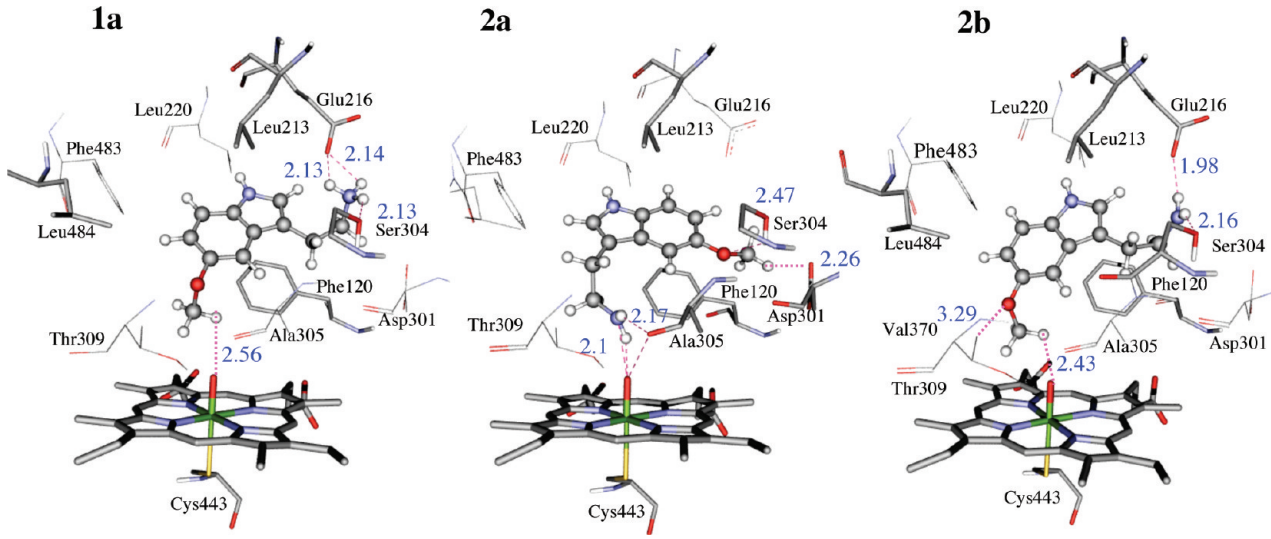

Figure 1. Most populated docking modes of the substrate 5-methoxytryptamine in the 2D6 protein. In protonated 5-MTH$^+$ (**1a**) the NH_3^+ tail is held by the negatively charged residues. In the nonprotonated 5-MT (**2a**), the unprotonated NH_2 faces toward FeO. A ball-and-stick model represents the substrate, and the interacting residues are shown as stick models.

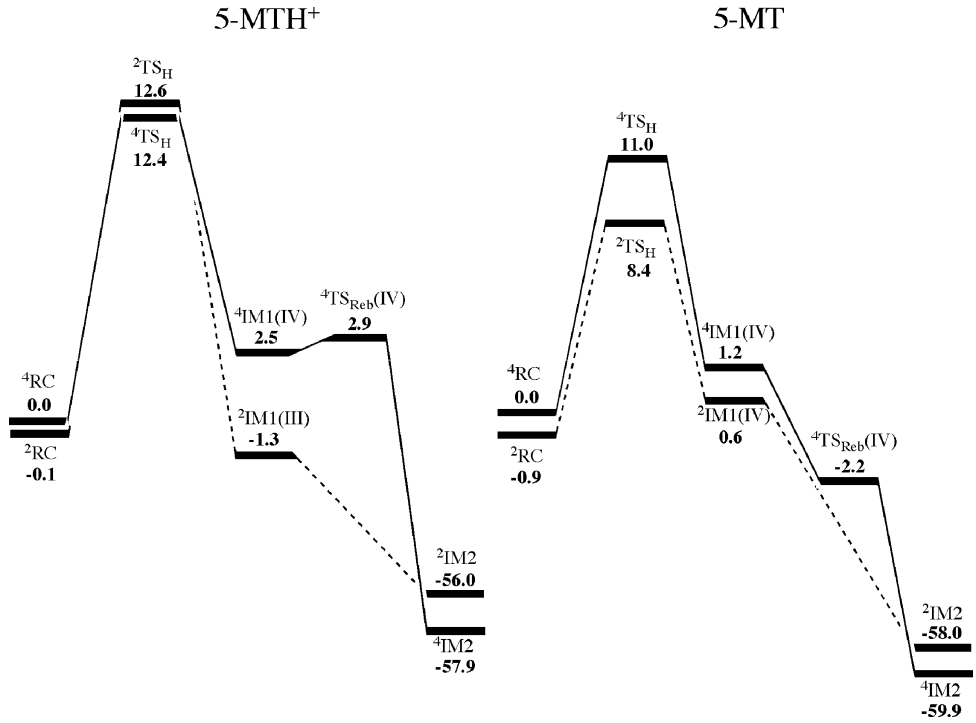

Figure 2. UB3LYP/B2 calculated energy profiles for hydroxylation of 5-MTH$^+$ and 5-MT by Cpd I. All energy data include ZPE correction and solvent ($\varepsilon = 5.6$).

Glu216, Asp301, and Phe120 have been reported earlier by both experimental[47−49] and docking studies[65−68] as important for the substrate binding in the 2D6 enzyme.

The 5-MT docking results show different conformations (**2a**, **2b**, and **2c**), two of which are shown in Figure 1. Conformation **2a** is oriented with the NH_2 tail maintaining H-bonding with the oxo group of Cpd I, whereas conformation **2b** is similar to **1a**. In other conformations, the substrate is not in the vicinity of the heme unit (see Supporting Information Figure S3). So unlike the protonated form 5-MTH$^+$, the uncharged 5-MT experiences less electrostatic interaction in the binding mode **2b**, which is similar to **1a**, and hence, the amino group can reorient toward the heme unit and act as an inhibitor in a similar way as discussed for dopamine formation and in drugs.[48,65−67] Furthermore, our DFT calculations for 5-MTH$^+$ show preference for the upright conformation, and therefore, we studied only the reactivity of this conformation.

Hydroxylation. Figure 2 shows the energy profiles for the hydroxylation reaction nascent from the LS and HS states, using two substrates that differ in the N-tail where 5-MTH$^+$ is protonated and 5-MT is nonprotonated. The first transition state, TS_H, corresponds to the hydrogen atom abstraction (H-abstraction) from the OMe group. This is then followed by hydroxyl rebound that produces the carbinol, IM2. The B1 barriers for rebound exist only for the HS states. At the B2 level, only 5-MTH$^+$ has a tiny barrier, and hence, the hydrogen atom transfer is rate-limiting for both 5-MTH$^+$ and 5-MT. Notwithstanding the small rebound barrier for 5-MTH$^+$, the reactions are effectively concerted on both states and give rise to the same oxidation products.

TABLE 1: Energies (kcal mol^{-1}), Calculated Relative to the RC Quartet (taken as zero), with the B2 Basis Set[a]

	5-MTH$^+$		5-MT	
	gas[b]	PCM[b,c]	gas[b]	PCM[b,c]
^{4}RC	0.0	0.0	0.0	0.0
^{2}RC	−0.2	−0.1	0.4	−0.9
^{4}TS$_H$	14.5	12.4	9.9	11.0
^{2}TS$_H$	16.3	12.6	8.9	8.4
^{4}IM1	2.4	2.5	0.1	1.2
^{2}IM1	5.3	−1.3	−0.4	0.6
^{4}TS2	4.7	2.9	0.2	−2.2
^{4}IM2	−51.9	−57.9	−57.3	−59.9
^{2}IM2	−52.7	−56.0	−58.4	−58.0

[a] The solvent contribution was calculated using PCM with the B2 basis set. [b] Including ZPE correction. [c] Including solvation contribution, using a solvent model with a dielectric constant, $\varepsilon = 5.6$.

Table 1 shows the relative energies at various levels. For comparison, more energies are presented in the Supporting Information, Tables S1−S4. Figures 3 and 4 display the key geometric parameters for each stationary point on these energy profiles. Figures 3 and 4 also show spin densities on the TS$_H$ species, and these spin density values (ρ) indicate clearly that the species involve iron in a IV oxidation state, Fe(IV), which is characterized by a total spin of close to 2.0 on the FeO moiety.[30] In addition, the amount of charge transfer in these transition states, Q_{CT}, shows that the substrate transfers a net of 0.25−0.27 electron to the heme-oxo moiety, leading to polar transition states.

The Hydrogen Atom Transfer Step. At our highest level (B2 + ZPE + solvation), the 5-MTH$^+$ activation energies for HS and LS transition states are 1.4 and 3.5 kcal mol^{-1} higher than the corresponding HS and LS barriers for 5-MT (Figure 2 and Table 1). However, without a bulk polarity contribution (see Table 1), these energy differences are larger. This intrinsic difference is decreased in a solvent environment due to screening of the NH_3^+ effect. Thus, as already mentioned above, the TS$_H$ species are polar, and as may be seen from Table 2, their dipole moments relative to the reactant cluster (RC) increase for the 5-MTH$^+$ substrate and slightly decrease for the 5-MT substrate. Therefore, inclusion of solvation stabilizes the TS$_H$(5-MTH$^+$) species more than the corresponding TS$_H$(5-MT) species.

As seen from Table 1 and Figure 3, for 5-MTH$^+$, the HS and LS states of the reactants and the transition states for the HAT reaction are not only almost degenerate in energy, but their geometries are also nearly the same. For both the HS and the LS species, the transition state is "late", meaning that the C−H distance is long and the H−O distance is short. A similar behavior is also observed for the HS species for 5-MT, but in this case, the C−H and H−O distances at the TS$_H$ are slightly shorter; see Figure 4. The ^{2}TS$_H$(5-MT) species, however, is

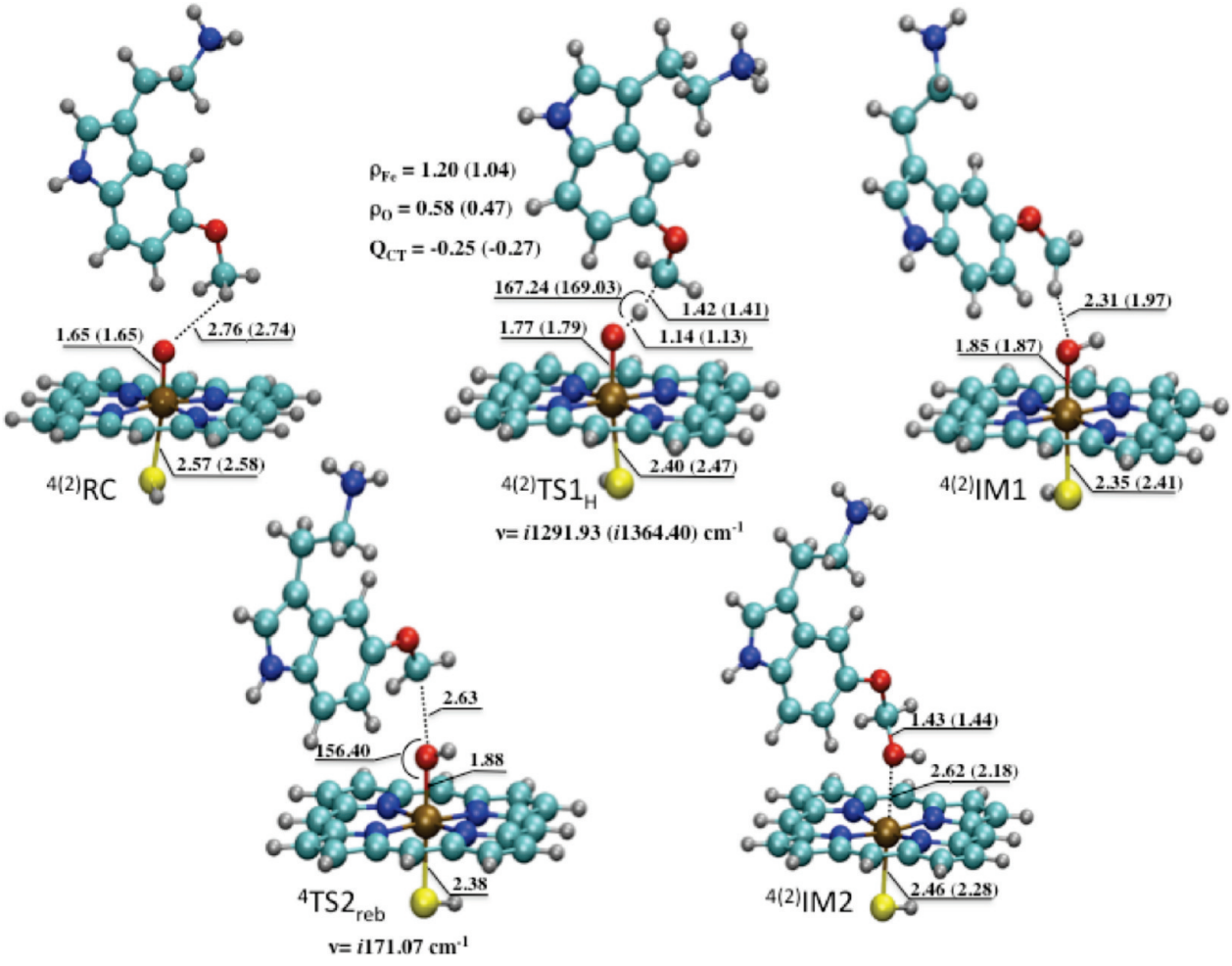

Figure 3. The UB3LYP/B1 calculated structures for the critical species during the hydroxylation of 5-MTH$^+$ by Cpd I. Each data set gives HS and LS values. The ^{2}IM1 structures are shoulders and not real intermediates. For $^{4(2)}$TS$_H$, we include the Fe and O spin densities (ρ) and the charge transferred from the substrate to the Cpd I moiety (Q_{CT}).

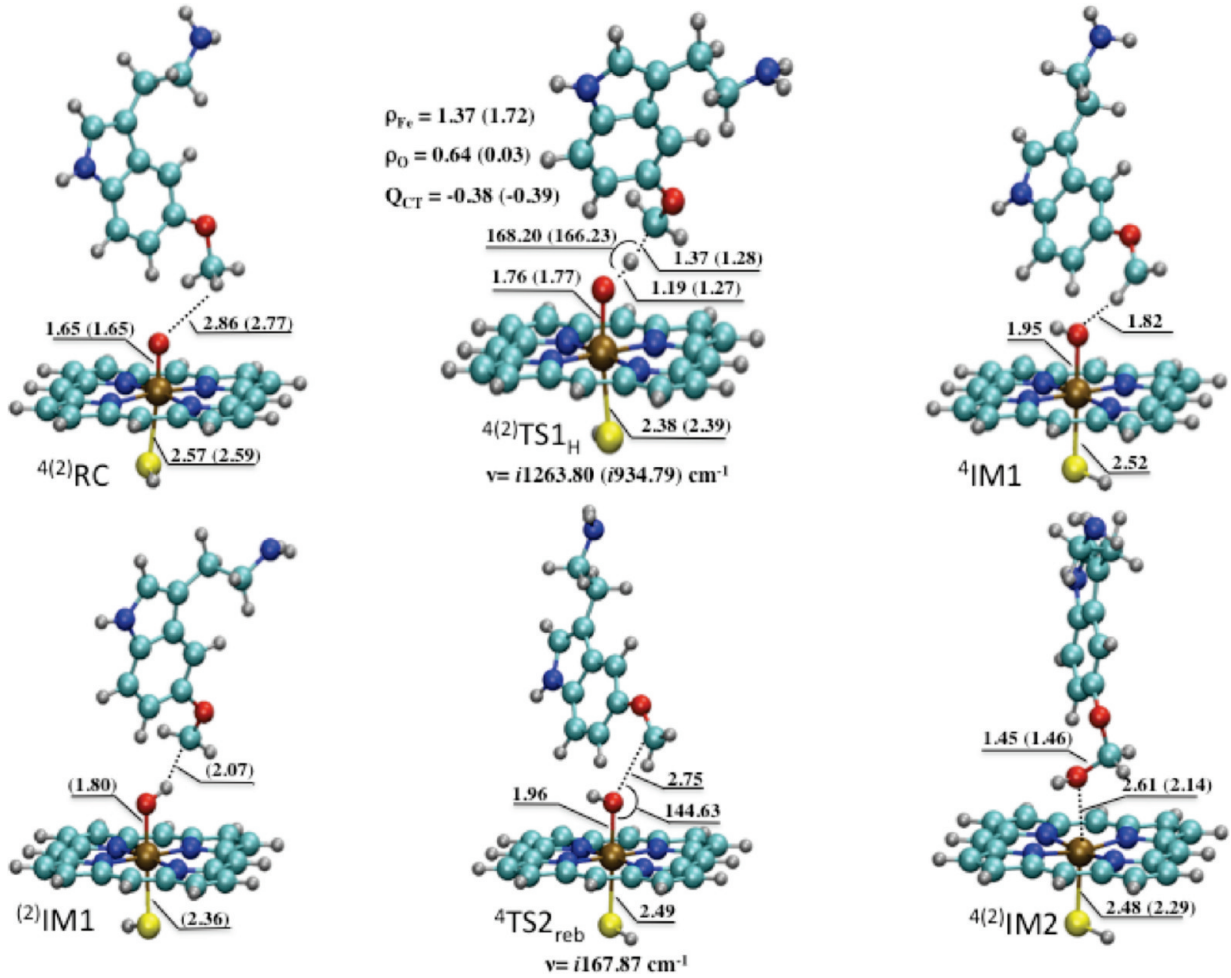

Figure 4. The UB3LYP/B1 calculated structures for the critical species during the hydroxylation of 5-MT by Cpd I. Each data set gives HS and LS values. The ^{2}IM1 structures are shoulders and not real intermediates.

TABLE 2: Relative Dipole Moment by Calculating the Change between TS_H and RC (Debye)

	5-MTH$^+$		5-MT	
	HS	LS	HS	LS
$\Delta\mu$	2.06	1.80	−0.79	−0.49

earlier, with the hydrogen centered between the C and the O, and in accordance with this, the corresponding energy barrier is lower.

The Effect of Glu216 on HAT. The substrate binding in the protein shows that Glu216 is interacting with the amino group of 5-MTH$^+$ and 5-MT (see Figure 1). The potential effect of the Glu216 interaction with the charged amino group of 5-MTH$^+$ on the HAT reaction was considered by including a carboxylate group in the DFT model. As seen in Table 3, the ^2TS_H(5-MTH$^+$ + Glu) energy is now barely affected when including a solvent. The ^2TS_H(5-MT + Glu) is more affected by the solvent, obviously because of the negative charge of the carboxylate group. Thus, the calculations of 5-MTH$^+$ + Glu show the same trend as the calculations without the carboxylate group in the DFT model and further justify our use of PCM to mimic a protein environment (for more details, see Supporting Information Tables S5 and S6).

In contrast to N-demethylation reactions, in which there is a longstanding debate whether the mechanism is initiated by HAT or SET, it is agreed that O-demethylation proceeds via HAT. Our calculated KIE values, in Table 4, are significant (5.5−6.4

TABLE 3: UB3LYP/B2 HAT Relative Energies (kcal mol^{-1}), Including a Glutamic Acid Residue and with Bulk Polarity Effects Using PCM

	5-MTH$^+$ + Glu		5-MT + Glu	
	gas[a]	PCM[a,b]	gas[a]	PCM[a,b]
^{2}RC	0.0	0.0	0.0	0.0
^2TS_H	13.9	13.3	17.0	11.5

[a] Including ZPE correction obtained without the carboxylate group, same as in Table 1. [b] Including solvation contribution, using a solvent model with a dielectric constant, $\varepsilon = 5.6$.

TABLE 4: B3LYP/B1 Computed KIEs[a]

	5-MTH$^+$	5-MT
KIE_{LS}	6.4 (8.6)	5.7 (6.8)
KIE_{HS}	6.4 (8.5)	6.3 (8.3)

[a] Values without parentheses refer to semiclassical Eyring KIEs, within parentheses are the Wigner-corrected KIEs.

using semiclassical Eyring KIEs, and with Wigner correction for tunneling the KIE's are even higher; see Methods section for more details), as might be expected from a HAT reaction. Experimental intramolecular KIE data for O-demethylation reactions that are of interest here are 9.4−9.6 for 7-methoxycoumarin, 6.1 for 7-ethoxycoumarin,[22] 7.3 for anisole,[69] 5.1[22] and 8.4 for 4-methoxyanisole, 7.0 for methacetin, and 8.4 for 4-cyanoanisole.[70]

The B2 basis set lowers all TS_H energy barriers, presumably reflecting the stabilization of the polar transition state by the

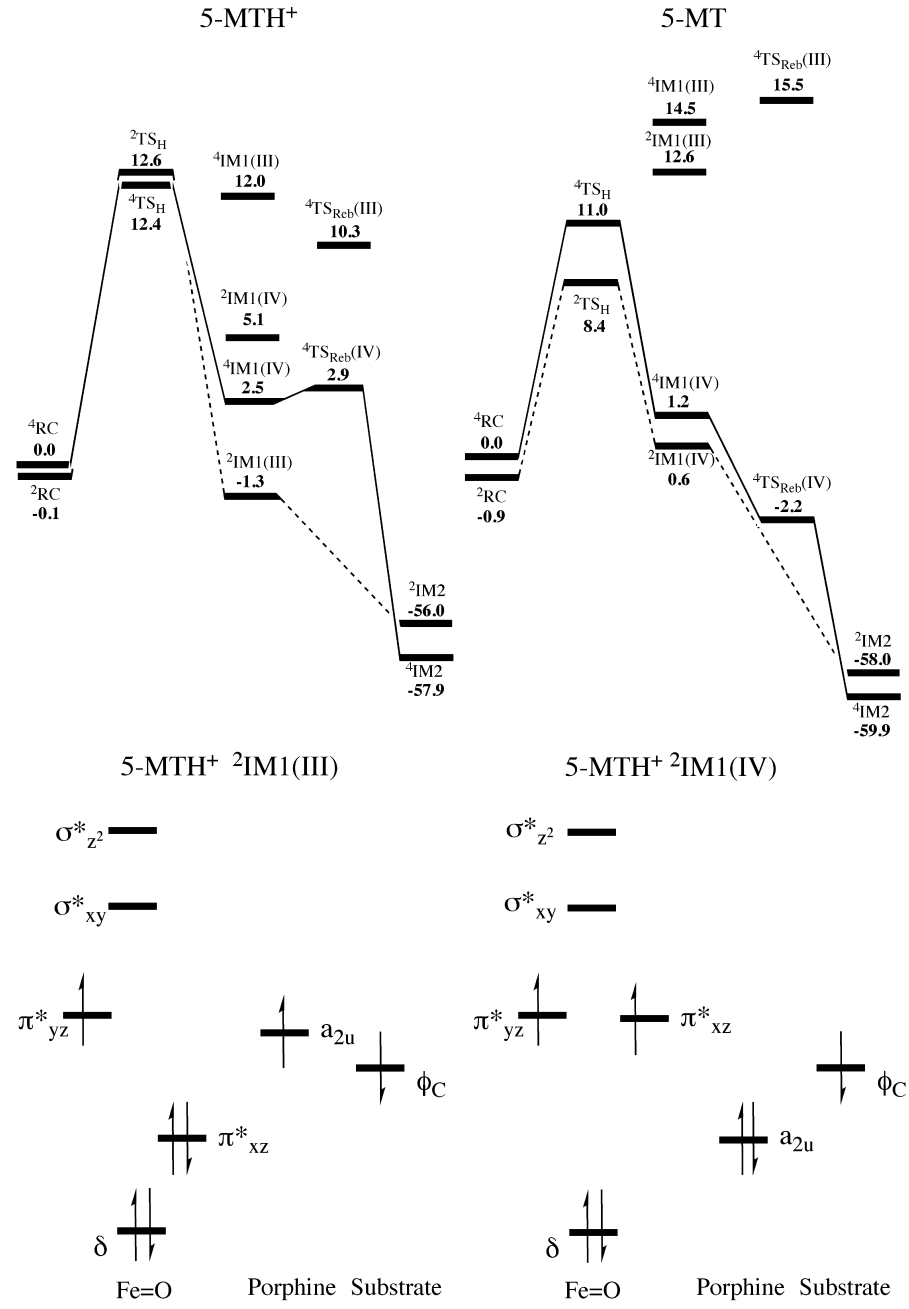

Figure 5. Energy profiles for hydroxylation of 5-MTH$^+$ and 5-MT by Cpd I, including the Fe(IV) and Fe(III) electromeric states of IM1. The energies are calculated with B2 basis set including ZPE and solvent ($\varepsilon = 5.6$) contributions. Shown below are the orbital occupation diagrams for the ^{2}IM varieties.

larger basis set,[71] as found in the analogous HAT in *N*,*N*-dimethylanilines.[64]

The Oxygen Rebound Mechanism: Formation of the Carbinol Intermediate. In the oxygen rebound step, the oxygen atom of the iron−hydroxo complex forms a bond with the CH_2 carbon of the substrate radical. The calculations with the B1 basis set generated $^4TS_{reb}$ species in the HS states for the two substrates. The imaginary frequencies for the $^4TS_{reb}$ species of the two substrates show that the transition state involves only a small reorientation of the CH_2 group to facilitate the bond formation. In both the 5-MT and 5-MTH$^+$ cases, the C−O distances at the $^4TS_{reb}$ species are long, 2.8 and 2.6 Å, respectively (see Figures 3 and 4). Furthermore, with B2 and solvent corrections, these rebound processes become barrier-free in all cases except for the HS state of 5-MTH$^+$, which still retains a small positive energy barrier.

The energies for the radical complexes (IM1) involved in the rebound process exhibit a large energy shift between B1 and B2 (Tables S2 and S4 in the Supporting Information). We verified that this large shift does not involve convergence of the two basis sets on different electromers of the IM1 intermediates, that is, Por$^{+\bullet}$Fe(III)OH/$^\bullet$CH$_2$R vs PorFe(IV)OH/$^\bullet$CH$_2$R (see Table S7 in the Supporting Information). We have further verified that the major contribution due to the energy decrease of the intermediates in B2 is common to the PorFe(IV)OH/$^\bullet$CH$_2$R electromer.[72]

The oxygen rebound reaction generates the carbinol intermediate, IM2. This intermediate is thermodynamically very stable as compared with RC (see Figure 2), with the HS states having the lowest energies.

Can both Fe(III) and Fe(IV) Species Be Involved in the Oxygen Rebound Reaction? Figure 2 contains ^{2,4}IM1 species in which iron belongs to the Fe(IV) variety in all cases except

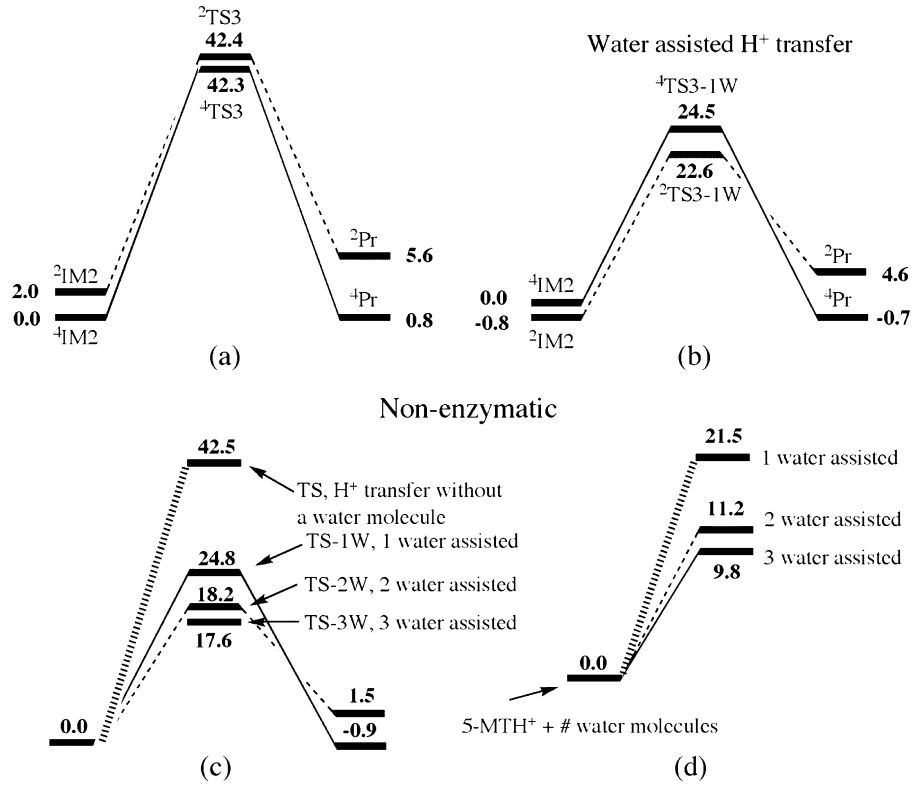

Figure 6. Energy profiles for carbinol decomposition, including water-assisted proton transfer (kcal mol^{-1}). The relative energies in parts a and b are calculated with a ferric carbinol complex in a solvent with $\varepsilon = 5.6$, whereas in part c, they are calculated for the free carbinol in an aqueous solution with $\varepsilon = 78.4$. In part d, the transition state energies are relative to the separately calculated water cluster and the carbinol (5-MTH$^+$). All data correspond to B2 energies.

for ^{2}IM1 of 5-MTH$^+$, which is an Fe(III) species. We therefore tested the potential involvement of the IM1 intermediates of Fe(III) and Fe(IV) varieties. We have to emphasize that except for ^{2}IM1(III), which is the ground state for the intermediates during HAT from 5-MTH$^+$, the other Fe(III) species could not be obtained with geometry optimization, and therefore, their energies are overestimated.

Figure 5 contains the B2 energy profiles in solvent for the hydroxylation reaction as presented in Figure 2 but with the addition of different electromeric species for the oxygen rebound reaction. The electronic structure diagrams in the figure show the different occupancies of Fe(III) and Fe(IV) species. The most significant change in the occupancy is that the π^*_{xz} orbital for Fe(III) is doubly occupied, whereas in the Fe(IV) case, one of these two electrons is transferred to the a_{2u} orbital. The major difference between the energy profiles for 5-MTH$^+$ and 5-MT substrates is that the preferred rebound reaction for ^{2}IM1(5-MTH$^+$) involves the Fe(III) electromer, whereas the electromer of the Fe(IV) variety is somewhat higher in energy. This feature reveals that the different protonation states of the two substrates change the access to the Fe(III) states (see also Table S9 in the Supporting Information). A recurring observation for the B2 energies is that the rebound barrier via ^{4}TS$_{reb}$(III) for 5-MTH$^+$, vanishes, as was previously observed for the ^{4}TS$_{reb}$(IV) 5-MT (see Figure 2).

In summary, Figure 5 shows that for 5-MTH$^+$ all the Fe(III) and Fe(IV) intermediates lie below the TS$_H$ species and are, hence, accessible during the reaction. In contrast, none of the Fe(III) intermediate states is accessible for the 5-MT substrate. Since in all cases, there are either tiny rebound barriers or none at all, this distinction may not have any practical effects.

Carbinol Decomposition. To complete the O-demethylation reaction, the O−C bond must be cleaved, and a hydrogen must rearrange its position (see Scheme 2). Figure 6 shows energy profiles for this final reaction step for the carbinol derived from 5-MTH$^+$, and more details can be found in Table 5. Figure 7 shows the corresponding transition state geometries, which involve H$^+$ migration/O−C cleavage.

TABLE 5: Energy Barriers for the Carbinol (5-MTH$^+$) Decomposition, Including ZPE[a]

	gas phase[b]	PCM[b,c]
	Heme + Water	
^{4}TS	44.4[d]	42.3
^{2}TS	44.7	42.4
^{4}TS-1W	22.4	24.5
^{2}TS-1W	24	22.6
	Nonenzymatic: 5-MTH$^+$ + Water	
TS	43.0[e]	42.5
TS-1W	24.2	24.8
TS-2W	16.5	18.2
TS-3W	15.4	17.6
5-MTH$^+$ + Water (TS relative completely dissociated water cluster)		
TS-1W	21.5[f]	
TS-2W	11.2	
TS-3W	9.8	

[a] All energies in kcal mol^{-1}. [b] Including ZPE corrections. [c] Including solvation contribution, using a solvent model with a dielectric constant, $\varepsilon = 5.6$ with the heme and $\varepsilon = 78.4$ for the nonenzymatic. [d] The energy barriers were calculated from the energy difference between the transition state and the ^{4}IM2. [e] The energy barriers were calculated from the energy difference between the transition state and the reactant complex. [f] The energy barriers were calculated from the energy difference between the transition state and the separately calculated energies of the water cluster and the carbinol.

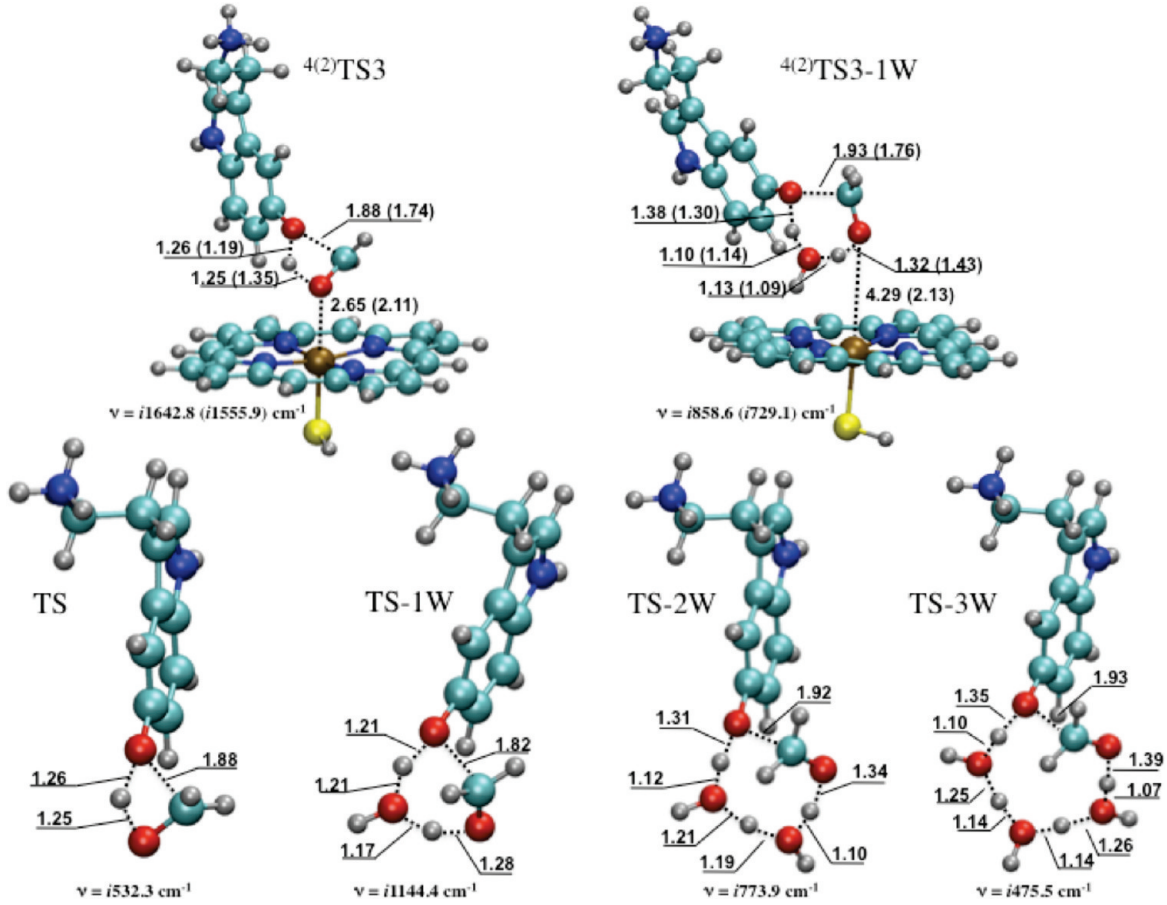

Figure 7. TS geometries for carbinol decomposition in the ferric complex and in the free form with and without water assistance.

The energy profiles in Figure 6a show the unassisted process from the IM2 ferric complexes. As expected,[64] the barrier for this proton migration/O−C cleavage is very high, >40 kcal mol^{-1}, and there is only a minor difference between the HS and LS states. The TS in Figure 7 has a four-membered ring structure and is hence strained. In a previous study of the N-demethylation reaction, a water molecule was shown to assist the proton transfer by relieving this strain in a six-membered ring structure.[64] This TS structure is shown in Figure 7, and the corresponding energy profile in Figure 6b shows that the barrier is reduced considerably to ∼23−25 kcal mol^{-1}. Still, this barrier is too high for what is considered to be a fast reaction, and as before,[64] more water molecules are required to reduce the barrier, but this requires that the reaction take place outside the active site, where water is more available.

As was shown before,[64] the binding free energy of the carbinol to the heme is significantly smaller than the barrier for the subsequent decomposition reaction so that it is most likely that the reaction will occur nonenzymatically in a detached carbinol molecule in an aqueous environment.[28] The lowering of the barrier with assisting water molecules supports the assumption that this reaction occurs outside the active site in a more aqueous environment. This and the result that the heme had little effect on the carbinol decomposition (see Table 5), enabled further exploration of the decomposition without the heme in an environment with a dielectric constant representing water.

The energy profiles in Figure 6c show the "non-water-molecule-assisted" and the water-molecule-assisted proton migration in the carbinol. In the case of "non-water-molecule-assisted" and one-water-molecule-assisted transfer, the energies are nearly the same as in the previous calculations, including the heme. The different protonation state of the substrate, protonated or neutral, had a minor effect on the carbinol decomposition; TS-1W(5-MT) has a barrier of 24.0 kcal mol^{-1} as compared with 24.8 kcal mol^{-1} for TS-1W(5-MTH$^+$) (Table S13 in SI). The energy diagrams also show the two- and three-water-molecule-assisted transfers, and it is seen that the barriers converge to ∼17−18 kcal mol^{-1}.

We also calculated the barriers for a gas phase process assisted by water clusters in Figure 6d. For the cases of two and three water molecules, a water cluster was initially optimized to take into account the water−water interaction energies. The barrier was determined relative to the separated reactants (carbinol and water clusters). The data in Figure 6d and Table 5 show that the barrier for the two-water-molecule-assisted reaction in the gas phase is 11.2 kcal mol^{-1}, and for the three-water-molecule-assisted reaction, the barrier is lowered to 9.8 kcal mol^{-1}. In principle, therefore, water clusters can catalyze the carbinol decomposition, but we cannot determine a precise barrier, which includes bulk aqueous solvent effects. What our calculations definitely show is that water molecules are needed to significantly lower the carbinol decomposition barrier, which is in accordance with experimental conclusions that this is a nonenzymatic process.[28]

4. Discussion

This paper describes the DFT study of the O-demethylation reaction of the trace amine 5-methoxytryptamine to produce the neurotransmitter serotonin. The different protonation states of the substrate, 5-MT and 5-MTH$^+$, have similar overall mechanisms but exhibit differences in details. In both cases, the initial

hydrogen atom abstraction from the substrate involves two spin states, followed by virtually barrier-free rebound to form the ferric−carbinol complexes. This is followed then by release of the carbinol and a water-assisted decomposition of the latter to yield serotonin and formaldehyde. A major difference between the two substrate forms is that the hydrogen abstraction barriers are larger for 5-MTH$^+$ and that this substrate may exhibit rebound with involvement of the Por$^{\bullet+}$Fe(III)OH and Por-Fe(IV)OH electromeric states and a small barrier for the latter electromer in the HS state. As explained later, however, we favor the scenario with the 5-MTH$^+$ substrate. It is also possible that the difference in reactivity between 5-MT and 5-MTH$^+$ will be reduced in a QM/MM study because of the electrostatic interaction between the protein residues and the substrate. An indication of this can be seen in Table 3, where a glutamic acid was added in the QM model and the ^2TS_H(5-MT + Glu) barrier is increased as compared with ^2TS_H(5-MT).

The computed energy barrier for the carbinol decomposition using a water−carbinol (5-MTH$^+$) complex (Figure 6c) corresponds, perhaps accidentally, to the experimentally obtained activation energy of 17.5 kcal mol^{-1} for the O-demethylation reaction by CYP2D6.[14] However, had this barrier been correct, the carbinol intermediate would have been most likely observable in the experiments, but such an observation during serotonin formation has not been reported, to the best of our knowledge. The data in Figure 6d indicate that in a real water environment, the carbinol decomposition barrier may be small.

The Regioselectivity of Oxidation. Let us return now to the question of the substrate's protonation state and the regioselectivity of oxidation. The issue of regioselectivity cannot be explained with our QM models, which lack the negatively charged protein residues, and hence, a better way would have been to perform QM/MM calculations[73] in which steric effects and electrostatic interactions of the protein are taken into account. Nevertheless, in our study, some quantitative assessments of these factors are still provided from the docking calculations, which complement the QM results. Thus, initially, there are a few potential regiochemical pathways for oxidation. One involves the O-demethylation; another involves hydroxylation of the CH_2NH_2 tail or N-oxidation at the amino end; and finally, another potential reaction is tryptophan hydroxylation at positions 4, 6, or 7 (Scheme 2).

C−H hydroxylation of the CH_2NH_2 tail of 5-MT should have a very small barrier[64] and could have well competed with the O-demethylation. The barrier for aromatic hydroxylation[74,75] is a bit on the high side. However, considering that the energy for the ring hydroxylation could be lowered[76] when the phenyl ring is part of a tryptophan skeleton and an $-OCH_3$ is substituted into the ring, the tryptophan hydroxylation may also compete with O-demethylation. However, experimentally,[14] CYP2D6 does not mediate 6-hydroxylation of 5-methoxytryptamine or, for that matter, O-demethylation of 6-methoxytryptamine and does not perform hydroxylation of the NH_2 tail. This remarkable observed selectivity for O-dealkylation suggests that the substrate's binding in the active site prevents free tumbling and leads to exclusive O-demethylation of 5-methoxytryptamine. As such, it appears that the protonation of 5-MT to 5-MTH$^+$ may be a decisive factor in the production of serotonin. Two amino acids of CYP2D6, Glu216, and Asp301 (especially the former),[47−49] which are located in the active site, hold the positively charged NH_3^+ group of 5-MTH$^+$ through electrostatic and hydrogen bonding interactions and orient the substrate in a perfect position to react with Cpd I by O-demethylation (**1a** in Figure 1). Experimentally,[48] it has been shown that the negative charges of Glu216 and Asp301 are crucial for the enzymatic activity, especially when the substrate has a charged amino group. It appears, therefore, that protonation of 5-MT to 5-MTH$^+$ serves an important function to optimize the yield of serotonin.

5. Conclusions

Cpd I of P450 effectively catalyzes the hydroxylation reaction of 5-methoxytryptamine in both protonation states but with a lower barrier for the neutral deprotonated 5-MT. The two protonation states, 5-MTH$^+$ and 5-MT, react differently with the Cpd I. The LS and HS states of Cpd I react with 5-MTH$^+$ without discriminating between the two spin states and lead thereby to a TSR scenario. The neutral 5-MT, on the other hand, has a clear preference for the LS over the HS, thus proceeding via a so-called single-state reactivity mechanism with a low barrier on the LS surface.[77] Consequently, even though the neutral 5-MT is not a substrate for the CYP2D6 enzyme, it is, in fact, the more reactive form of 5-methoxytryptamine. These results in combination with substrate binding in the protonated form ensure a highly regioselective hydroxylation for an optimal serotonin yield.

In the last reaction step of the O-demethylation, the carbinol decomposition occurs in an aqueous environment and is assisted by at least two or three water molecules. The present result, that more than two water molecules are needed to lower the barrier significantly, rules out that the reaction is enzymatic and occurring in the largely hydrophobic active site. Since it seems to require an aqueous medium, it is likely that the reaction occurs outside the active site within the aqueous medium.

Acknowledgment. The paper is dedicated to Henry (Fritz) Schaefer, for his seminal contributions to computational quantum chemistry, on the occasion of his forthcoming 65th birthday. The research was supported by an ISF Grant, 53/09, to S.S. P.S. thanks The Wenner-Gren Foundation for a fellowship to work in Jerusalem on brain chemistry.

Supporting Information Available: Energies and electronic features are presented in tables, and *xyz* coordinates are given for various reaction species discussed in the paper. The SI document also contains the detailed docking methodology and analyses of 5-methoxytryptamine. This material is available free of charge via the Internet at http://pubs.acs.org.

References and Notes

(1) Porter, T. D.; Coon, M. J. *J. Biol. Chem.* **1991**, *266*, 13469–13472.
(2) Coon, M. J. *Annu. Rev. Pharmacol. Toxicol.* **2005**, *45*, 1–25.
(3) (a) *Cytochrome P450: Structure, Mechanisms, and Biochemistry*, 2nd ed.; Ortiz de Montellano, P. R., Ed.; Plenum Press: New York, 1995. (b) *Cytochrome P450: Structure, Mechanism, and Biochemistry*, 3rd ed.; Ortiz de Montellano, P. R., Ed.; Kluwer Academic/Plenum: New York, 2005.
(4) Groves, J. T. *Models and Mechanisms of Cytochrome P450 Action Cytochrome P450: Structure, Mechanism, and Biochemistry*, 3rd ed.; Ortiz de Montellano, P. R., Ed.; Kluwer Academic/Plenum: New York, 2005, pp 1−43.
(5) Sono, M.; Roach, M. P.; Coulter, E. D.; Dawson, J. H. *Chem. Rev.* **1996**, *96*, 2841–2887.
(6) The Ubiquitous Role of Cytochrome P450 Proteins. In *Metal Ions in Life Sciences*; Sigel, A., Sigel, H. , Sigel, R. K. O., Eds.; John Wiley & Sons Ltd: Chichester, England, 2007; Vol. 3.
(7) Guengerich, F. P. In *Cytochrome P450: Structure, Mechanism, and Biochemistry*, 2nd ed.; Ortiz de Montellano, P. R. , Ed.; Academic/Plenum Press: New York, 2005, pp 473−535.
(8) (a) Guengerich, F. P. *Annu. Rev. Pharmacol. Toxicol.* **1999**, *39*, 1–17. (b) Munro, A. W.; Girvan, H. M.; McLean, K. J. *Nat. Prod. Rep.* **2007**, *24*, 585–609.

(9) Zanger, U. M.; Raimundo, S.; Eichelbaum, M.; Schmiedebergs, N. *Arch. Pharmacol.* **2004**, *369*, 23–37.
(10) Guengerichrich, F. P. In *Cytochrome P450: Structure, Mechanisms, and Biochemistry*, 2nd ed.; Ortiz de Montellano, P. R. , Ed.; Plenum Press: New York, 1995.
(11) Evans, W. E.; Relling, M. V. *Science* **1999**, *286*, 487–491.
(12) Haining, R. L.; Nichols-Haining, M. *Pharmacol. Ther.* **2007**, *113*, 537–545.
(13) Burchett, S. A.; Hicks, T. P. *Prog. Neurobiol.* **2006**, *79*, 223–246.
(14) Yu, A.-M.; Idle, L. J.; Byrd, L. G.; Krausz, K. W.; Küpfer, A.; Gonzalez, F. J. *Pharmacogenet. Genomics* **2003**, *13*, 173–181.
(15) Patel, S.; Dulluc, J.; Geffard, M. *Histochemistry* **1986**, *85*, 259–263.
(16) Weissman, S. A.; Zwege, D. *Tetrahedron* **2005**, *61*, 7833–7863.
(17) Cnubben, N. H. P.; Vervoort, J. V. C.; Rietjens, I. M. C. M. *Chem. Biol. Interact.* **1992**, *85*, 151–172.
(18) Guengerich, F. P.; Macdonald, T. L. *FASEB J.* **1990**, *4*, 2453–2459.
(19) Guengerich, F. P.; Macdonald, T. L. *Adv. Electron Transfer Chem.* **1993**, *3*, 191–241.
(20) Watanabe, Y.; Oae, S.; Iyanagi, T. *Bull. Chem. Soc. Jpn.* **1982**, *55*, 188–195.
(21) Guengerich, F. P.; Miller, G. P.; Hanna, I. H.; Sato, H.; Martin, M. V. *J. Biol. Chem.* **2002**, *277*, 33711–33719.
(22) Kim, K.-H.; Isin, E. M.; Yun, C. H.; Kim, D. H.; Guengerich, F. P. *FEBS J.* **2006**, *273*, 2223–2231.
(23) (a) Miwa, G. T.; Walsh, J. S.; Kedderis, G. L.; Hollenberg, F. P. *J. Biol. Chem.* **1983**, *258*, 14445–14449. (b) Miwa, G. T.; Garland, W. A.; Hodshon, B. J.; Lu, A. Y. H.; Northrop, D. B. *J. Biol. Chem.* **1980**, *255*, 6049–6054.
(24) Abdel-Monem, M. M. *J. Med. Chem.* **1975**, *18*, 427–430.
(25) Hollenberg, P. F.; Miwa, G. T.; Walsh, J. S.; Dwyer, L. A.; Kedderis, G. L. *Drug Metab. Dispos.* **1985**, *13*, 272–275.
(26) Guengerich, F. P.; Yun, C.-H.; Macdonald, T. L. *J. Biol. Chem.* **1996**, *271*, 27321–27329.
(27) See, however, a criticism of this mechanistic criteria for SET: (a) Dinnocenzo, J. P.; Karki, S. B.; Jones, J. P. *J. Am. Chem. Soc.* **1993**, *115*, 7111–7116. (b) Karki, S. B.; Dinnocenzo, J. P.; Jones, J. P.; Korzekwa, K. R. *J. Am. Chem. Soc.* **1995**, *117*, 3657–3664. (c) Manchester, J. I.; Dinnocenzo, J. P.; Higgins, L. A.; Jones, J. P. *J. Am. Chem. Soc.* **1997**, *119*, 5069–5070.
(28) Nassar, A. F.; Hollenberg, P. F.; Scatina, J. *Drug Metabolism Handbook: Concept and Application*; John Wiley & Sons, Inc.: Hoboken, NJ, 2009.
(29) Meunier, B.; de Visser, S. P.; Shaik, S. *Chem. Rev.* **2004**, *104*, 3947–3980.
(30) Shaik, S.; Kumar, D.; de Visser, S. P.; Altun, A.; Thiel, W. *Chem. Rev.* **2005**, *105*, 2279–2328.
(31) Denisov, I. G.; Makris, T. M.; Sligar, S. G.; Schlichting, I. *Chem. Rev.* **2005**, *105*, 2253–2277.
(32) Dowers, T. S.; Rock, D. A.; Jones, J. P. *J. Am. Chem. Soc.* **2004**, *126*, 8868–8869.
(33) Ortiz de Montellano, P. R.; de Voss, J. J. *Nat. Prod. Rep.* **2002**, *19*, 477–493.
(34) Groves, J. T. *J. Chem. Educ.* **1985**, *62*, 928–931.
(35) Dowers, T. S.; Jones, J. P. *Drug Metab. Dispos.* **2006**, *34*, 1288–1290.
(36) Li, C.; Wu, W.; Kumar, D.; Shaik, S. *J. Am. Chem. Soc.* **2006**, *128*, 394–395.
(37) Shaik, S.; Hirao, H.; Kumar, D. *Acc. Chem. Res.* **2007**, *40*, 532–542.
(38) Kumar, D.; de Visser, S. P.; Sharma, P. K.; Cohen, S.; Shaik, S. *J. Am. Chem. Soc.* **2004**, *126*, 1907–1920.
(39) Guengerich, F. P. In *Advances in Drug Metabolism in Man*; Pacifici, G. M., Fracchia, G. N., Eds.; ECSC-EC-EAEC: Brussels, 1995, pp 180−231.
(40) Ekins, S.; de Groot, M. J.; Jones, J. P. *Drug Metab. Dispos.* **2001**, *29*, 936–944.
(41) Wolff, T.; Distlerath, L. M.; Worthington, M. T.; Groopman, J. D.; Hammons, G. J.; Kadlubar, F. F.; Prough, R. A.; Martin, M. V.; Guengerich, F. P. *Cancer Res.* **1985**, *45*, 2116–2122.
(42) Islam, S. A.; Wolf, C. R.; Lennard, M. S.; Sternberg, M. J. E. *Carcinogenisis* **1991**, *12*, 2211–2219.
(43) Koymans, L. M. H.; Vermeulen, N. P. E.; van Acker, S. A. B. E.; te Koppele, J. M.; Heykants, J. J. P.; Lavrijsen, K.; Meuldermans, W.; Donné-Opdenkelder, G. M. *Chem. Res. Toxicol.* **1992**, *5*, 211–219.
(44) Strobl, G. R.; von Kruedener, S.; Stockigt, J.; Guengerich, F. P.; Wolff, T. *J. Med. Chem.* **1993**, *36*, 1136–1145.
(45) Meyer, U. A.; Gut, J.; Kronbach, T.; Skoda, C.; Meier, U. T.; Catin, T.; Dayer, P. *Xenobiotica* **1986**, *16*, 449–464.
(46) Miller, G. P.; Hanna, I. H.; Nishimura, Y.; Guengerich, F. P. *Biochemistry* **2001**, *40*, 14215–14223.
(47) Ellis, S. W.; Hayhurst, G. P.; Smith, G.; Lightfoot, T.; Wong, M. M. S.; Simula, A. P.; Ackland, M. J.; Sternberg, M. J. E.; Lennard, M. S.; Tucker, G. T.; Wolf, C. R. *J. Biol. Chem.* **1995**, *270*, 29055–29068.
(48) (a) Paine, M. J.; McLaughlin, L. A.; Flanagan, J. U.; Kemp, C. A.; Sutcliffe, M. J.; Roberts, G. C. K.; Wolf, C. R. *J. Biol. Chem.* **2003**, *278*, 4021–4027. (b) Guengerich, F. P.; Hanna, I. H.; Martin, M. V.; Gillam, E. M. J. *Biochemistry* **2003**, *42*, 1245–1253.
(49) Rowland, P.; Blaney, F. E.; Smyth, M. G.; Jones, J. J.; Leydon, V. R.; Oxbrow, A. K.; Lewis, C. J.; Tennant, M. G.; Modi, S.; Eggleston, D. S.; Chenery, R. J.; Bridges, A. M. *J. Biol. Chem.* **2006**, *281*, 7614–7622.
(50) AUTODOCK, 10550, North Torrey Pines Road, La Jolla, CA 92037-1000.
(51) (a) Collins, J. R.; Camper, D. L.; Loew, G. H. *J. Am. Chem. Soc.* **1991**, *113*, 2736–2743. (b) Harris, D.; Loew, G. H. *J. Am. Chem. Soc.* **1995**, *117*, 2738–2746.
(52) (a) Favia, A. D.; Cavalli, A.; Masetti, M.; Carotti, A.; Recanatini, M. *Proteins Struct., Funct., Bioinf.* **2006**, *62*, 1074–1087. (b) Seifert, A.; Tatzel, S.; Schmid, R. D.; Pleiss, J. *Proteins Struct. Funct., Bioinf.* **2006**, *64*, 147–155.
(53) Morris, G. H.; Goodshell, D. S.; Halliday, R. S.; Huey, R.; Hart, W. E.; Belew, R. K.; Olson, A. J. *J. Comput. Chem.* **1998**, *19*, 1639–1662.
(54) Hu, X.; Balaz, S.; Shelver, W. H. *J. Mol. Graph. Model.* **2004**, *22*, 293–307.
(55) Frisch, M. J.; Trucks, G. W.; Schlegel, H. B.; Scuseria, G. E.; Robb, M. A.; Cheeseman, J. R.; Montgomery, J. A., Jr.; Vreven, T.; Kudin, K. N.; Burant, J. C.; Millam, J. M.; Iyengar, S. S.; Tomasi, J.; Barone, V.; Mennucci, B.; Cossi, M.; Scalmani, G.; Rega, N.; Petersson, G. A.; Nakatsuji, H.; Hada, M.; Ehara, M.; Toyota, K.; Fukuda, R.; Hasegawa, J.; Ishida, M.; Nakajima, T.; Honda, Y.; Kitao, O.; Nakai, H.; Klene, M.; Li, X.; Knox, J. E.; Hratchian, H. P.; Cross, J. B.; Bakken, V.; Adamo, C.; Jaramillo, J.; Gomperts, R.; Stratmann, R. E.; Yazyev, O.; Austin, A. J.; Cammi, R.; Pomelli, C.; Ochterski, J. W.; Ayala, P. Y.; Morokuma, K.; Voth, G. A.; Salvador, P.; Dannenberg, J. J.; Zakrzewski, V. G.; Dapprich, S.; Daniels, A. D.; Strain, M. C.; Farkas, O.; Malick, D. K.; Rabuck, A. D.; Raghavachari, K.; Foresman, J. B.; Ortiz, J. V.; Cui, Q.; Baboul, A. G.; Clifford, S.; Cioslowski, J.; Stefanov, B. B.; Liu, G.; Liashenko, A.; Piskorz, P.; Komaromi, I.; Martin, R. L.; Fox, D. J.; Keith, T.; Al-Laham, M. A.; Peng, C. Y.; Nanayakkara, A.; Challacombe, M.; Gill, P. M. W.; Johnson, B.; Chen, W.; Wong, M. W.; Gonzalez, C.; Pople, J. A. *Gaussian 03, Rev D.01*; Gaussian, Inc., Wallingford CT, 2004.
(56) Ogliaro, F.; Harris, N.; Cohen, S.; Filatov, M.; de Visser, S. P.; Shaik, S. *J. Am. Chem. Soc.* **2000**, *122*, 8977–8989.
(57) de Visser, S. P.; Ogliaro, F.; Sharma, P. K.; Shaik, S. *J. Am. Chem. Soc.* **2002**, *124*, 11809–11826.
(58) Becke, A. D. *J. Chem. Phys.* **1992**, *97*, 9173–9177.
(59) Becke, A. D. *J. Chem. Phys.* **1993**, *98*, 5648–5652.
(60) Lee, C.; Yang, W.; Parr, R. G. *Phys. Rev. B* **1988**, *37*, 785–789.
(61) Hay, P. J.; Wadt, W. R. *J. Chem. Phys.* **1985**, *82*, 299–310.
(62) Friesner, R. A.; Murphy, R. B.; Beachy, M. D.; Ringnalda, M. N.; Pollard, W. T.; Dunietz, B. D.; Cao, Y. *J. Phys. Chem. A* **1999**, *103*, 1913–1928.
(63) Melander, L.; Saunders, H. W., Jr. In *Reaction Rates of Isotopic Molecules*; Robert, E. Krieger Publishing Company: Malabar, 1987.
(64) Wang, Y.; Kumar, D.; Yang, C.; Han, K.; Shaik, S. *J. Phys. Chem. B* **2007**, *111*, 7700–7710.
(65) (a) Ito, Y.; Kondo, H.; Goldfarb, P. S.; Lewis, D.V. F. *J. Mol. Graph. Model.* **2008**, *26*, 947–956. (b) de Graaf, C.; Oostenbrink, C.; Keizers, B. M. A.; Vugt-Lussenburg, V.; van Waterschoot, R. A. B.; Tschirret-Guth, R. A.; Commandeur, J. N. M.; Vermeulen, N. P. E. *Curr. Drug Metab.* **2007**, *8*, 59. (c) Keizers, P. H. J.; de Graaf, C.; de Kanter, F. J. J.; Oostenbrink, C.; Feenstra, K. A.; Commandeur, J. N. M.; Vermeulen, N. P. E. *J. Med. Chem.* **2005**, *48*, 6117–6127.
(66) (a) Maréchal, J.-D.; Kemp, C. A.; Roberts, G. C. K.; Wolf, C. R.; Sutcliffe, M. J. *Br. J. Pharmacol.* **2008**, *153*, S82–S89. (b) Oostenbrink, C.; Ruiter de, A.; Hritz, J. *J. Med. Chem.* **2008**, *518*, 7469–7477.
(67) (a) Costache, A. D.; Trawick, D.; Bohl, D.; Sem, D. S. *Xenobiotica* **2007**, *37*, 221–245. (b) Saraceno, M.; Coi, A.; Bianucci, A. M. *Int. J. Biol. Macromol.* **2008**, *42*, 363–371.
(68) (a) McLaughlin, L. A.; Paine, M. J. I.; Maréchal, J.-D.; Flanagan, J. U.; Ward, C. J.; Sutcliffe, M. J.; Roberts, G. C. K.; Wolf, C. R. *J. Biol. Chem.* **2005**, *280*, 38617–38624. (b) Yu, J.; Paine, M. J. I.; Maréchal, J.-D.; Kemp, C. A.; Ward, C. J.; Brown, B.; Sutcliffe, M. J.; Roberts, G. C. K.; Rankin, E. M.; Wolf, C. R. *Drug Metab. Dispos.* **2006**, *34*, 1386–1392.
(69) Lindsay-Smith, J. R.; Sleath, P. R. *J. Chem. Soc., Perkin Trans. 2* **1983**, 621–628.
(70) Guengerich, F. P.; Krauser, J. A.; Johnson, W. W. *Biochemistry* **2004**, *43*, 10775–10788.
(71) Shaik, S.; Kumar, D.; de Visser, S. P. *J. Am. Chem. Soc.* **2008**, *130*, 10128–10140.
(72) Shaik, S.; Cohen, S.; de Visser, S. P.; Sharma, P. K.; Kumar, D.; Kozuch, S.; Ogliaro, F.; Danovich, D. *Eur. J. Inorg. Chem.* **2004**, *20*, 7–226.

(73) For a recent review on QM/MM calculations with P450, see: Shaik, S.; Cohen, S.; Wang, Y.; Chen, H.; Kumar, D.; Thiel, W. *Chem. Rev.* **2010**, *110*, 949–1017.
(74) de Visser, S. P.; Shaik, S. *J. Am. Chem. Soc.* **2003**, *125*, 7413–7424.
(75) Bathelt, C. M.; Mulholland, A. J.; Harvey, J. N. *J. Phys. Chem. A* **2008**, *112*, 13149–13156.
(76) (a) Rydberg, P.; Ryde, U.; Olsen, L. *J. Phys. Chem. A* **2008**, *112*, 13058–13065. (b) de Visser, S. P. *Chem.—Eur. J.* **2006**, *12*, 8168–8177.
(77) Schröder, D.; Shaik, S.; Schwarz, H. *Acc. Chem. Res.* **2000**, *33*, 139–145.

JP1008994